The rupture and independent extension of sister membranes in *C. elegans* embryos

Jingjing Liang[1]*, Tingrui Huang[1,2,3], Xun Huang[1,2], and Mei Ding[1,2]*

[1] Institute of Genetics and Developmental Biology, Chinese Academy of Sciences, Beijing 100101, China

[2] Taikang Center for Life and Medical Sciences, School of Basic Medical Sciences, Wuhan University, Wuhan 430071, China

[3] University of Chinese Academy of Sciences, Beijing 100049, China

* Correspondence: jjliang@genetics.ac.cn; mding@genetics.ac.cn

Abstract

Cytokinesis, the physical separation of a cell into two daughter cells, is classically thought to require continuous plasma membrane invagination driven by equatorial contractile forces. Here, we challenge this paradigm by uncovering an unexpected mechanism in *C. elegans* embryos: the plasma membrane ruptures as early as metaphase, detaching sister membranes before cytokinesis begins. Instead of invaginating as a continuous sheet, the separated membranes extend independently to partition the cytoplasm. This separation creates membrane discontinuities—widely observed in electron microscopy (EM) sections—both between the sister membranes and within individual sister cells. The exposed cytoplasmic regions are shielded by extracellular matrix components, likely preventing massive leakage. Our findings overturn the long-standing assumption that cytokinesis requires persistent membrane integrity, and offer fresh insights into cell division.

Introduction

In animal cells, the first visible sign of cytokinesis is the appearance of a cleavage furrow on the cell surface, which progressively deepens until the cell divides into two daughter cells (Fig1. A). Classical models universally presume that cytokinesis is executed beneath an intact plasma membrane, driven by a contractile ring of actin filaments, myosin II, and regulatory proteins (*1*), with vesicle fusion supplying new membrane to accommodate shape change (*2*). Critically, the foundational premise of uninterrupted membrane integrity during cytokinesis has never been rigorously tested until our unexpected discovery in *C. elegans* embryos.

During the early development of the nematode *C. elegans*, cells undergo rapid division (15-30 minutes per cycle), with each cycle alternating between S (DNA synthesis) and M (mitosis and cytokinesis) phases while bypassing G1/G2 until the 28-cell stage (*3–7*). During routine ultrastructural analysis, we made a startling observation that contradicts textbook models: rather than maintaining membrane continuity, embryonic cells routinely exhibit plasma membrane rupture as early as metaphase. Further analysis revealed that cytokinesis primarily occurs through independent extension of unconnected sister membranes (Fig. 1B), a mechanism never before documented.

This discovery challenges the canonical view of cytokinesis at its core, revealing an unanticipated plasticity in cell division mechanisms and prompting a re-evaluation of how membrane dynamics are regulated across species.

Results

Widespread membrane discontinuities in dividing *C. elegans* embryonic cells

In *C. elegans*, early-stage embryos remain inside the adult hermaphrodite until reaching approximately the 28-cell stage (the onset of gastrulation), after which they are laid (fig. S1). By examining the entire circumference of 425 cells in single high-pressure freezing transmission electron microscopy (HPF-TEM) sections (fig. S1) (*8*), we were surprised to find membrane discontinuities or gaps in 159 cells distributed across 57 embryos, representing 95% of the total sampled embryos (Fig. 1C). Among these 159 affected cells, 89% (141/159) exhibited a single membrane discontinuity (hereafter termed membrane opening, MO), while 13 cells had two openings and 5 cells had three. MO-containing cells were observed in laid embryos (fig. S2). However, as the embryos approached comma stage (*5*), which marks the onset of elongation (fig. S1), the frequency of MOs decreased dramatically (see Methods and Materials for details of all the stages examined).

A defining characteristic of early *C. elegans* embryonic cells is their rapid and extensive cell division. Within approximately 100 minutes, a two-cell embryo develops into an embryo containing nearly 30 cells (*6*). Given this dynamic proliferation, we hypothesized that the formation of membrane discontinuities might be associated with cell division events. To investigate this possibility, we analyzed the 159 cells exhibiting MOs based on nuclear and cytoplasmic morphology (Fig. 1C). Of these, 64 cells appeared in EM sections containing only cytoplasmic regions—9 of which completely lacked discernible plasma membranes. The remaining 95 cells contained one or more nuclei or condensed chromosomes. Among them, 10 cells were clearly in metaphase stage (defined by a single chromosomal cluster). As shown in Fig. 1D, a representative metaphase cell (MC) displayed a MO (dashed white line)

spanning roughly one-third of the cell's circumference. High-magnification imaging revealed that in contrast to the wrinkled plasma membranes (Fig. 1D, enlarged boxed area displayed in 1), the large MO exhibited a smoother surface morphology, and the internal cytoplasm remained enclosed within the cell (Fig. 1D, enlarged boxed areas displayed in 2 and 3). MOs were also observed in anaphase cells (AC) (n=5; characterized by <10 chromosomal clumps; Fig. 1E, enlarged in 2) and telophase cells (n=5; defined by two nuclei sharing cytoplasm; fig. S3). Intriguingly, one telophase-like cell contained three nuclei within a common cytoplasm (fig. S1, marked by &).

Because EM sectioning captures cells at random stages of the cell cycle, we sought to systematically assess the relationship between mitosis and MOs. To do so, we analyzed 20 cells with unambiguous division features, selected based on nuclear morphology—such as aligned chromosomes (metaphase) or discrete clusters (anaphase)—and cytoplasmic sharing, indicated by two or more nuclei within a common cytoplasm (telophase). Strikingly, 19 out of 20 cells (95%) revealed MOs upon tracing the plasma membrane in single EM sections (fig. S3). This near-ubiquitous association strongly suggests that membrane discontinuities are an integral feature of cell division in early *C. elegans* embryos.

Membrane rupture in cells at metaphase

The observed membrane discontinuities suggest that the plasma membrane of early *C. elegans* embryos may rupture during cell division. However, because TEM provides only static, two-dimensional images, we could not determine the three-dimensional nature of these ruptures. To better understand this phenomenon, we acquired continuous serial sections and performed 3D reconstruction.

Since membrane discontinuities appear as early as metaphase—well before nuclear or cytoplasmic division—we performed continuous EM sectioning to trace the entire plasma membrane of a metaphase cell (Fig. 2, A to C). Through 3D reconstruction, we identified a continuous plasma membrane rupture extending over 8,940 nm, which is more than two-thirds of the cell's circumference (Fig. 2, D). Notably, one end of the membrane rupture appeared long and narrow, while the other was wide and exhibited cytoplasmic leakage (Fig. 2, D). Further analysis revealed that the leaked cytoplasm remained confined to a relatively localized region (Fig. 2, B and Movie S1). During metaphase, chromosomes align at the equatorial plane, a key region for subsequent segregation. To explore the spatial relationship between membrane rupture and chromosomal organization, we further reconstructed the entire condensed chromosome region. We found that this large-scale membrane rupture largely encircled the chromosomal disc (Fig. 2D and Movie S1), spatially aligning with the future segregation zone.

The detachment of sister membranes

According to the conventional model, cytokinesis in animal cells begins with the formation of a membrane invagination. As this invagination deepens, it gives rise to two back-to-back membrane layers, ultimately leading to the physical separation of the two daughter cells. In the context of membrane rupture, however, plasma membrane disruption results in the separation of two putative sister membranes—likely as early as metaphase. We then asked how the subsequent cytokinesis process proceeds with detached sister membranes. To address this question, we examined 51 dividing cells. In each of these cells, two well-separated nuclei were observed, indicating that they were at telophase. We found that while a minority of cells (6/51)

exhibited classical membrane invagination (Fig. 3A), including one embryo transitioning from the one-cell to the two-cell stage, the vast majority (45/51) displayed a striking detached membrane configuration (Fig. 3B). In these cases, sister membrane tips were completely separated from each other (Fig. 3, B and C, marked with *), forming distinct, non-contiguous structures that defy conventional models of cytokinesis. This predominant pattern suggests that membrane detachment—rather than continuous invagination—may represent the primary mode of cytoplasmic separation in *C. elegans* embryos. Of note, the membrane rupture simultaneously generates individual sister membranes with severed edges. Indeed, as shown in Fig. 3B, the tips of both free-ended edges (*) of Cell 1 are visible in the EM section.

In the detached membrane configuration, cytoplasmic components—such as glycogen granules and ribosomal particles—were clearly visible surrounding the severed edges of the two sister membranes (Fig. 3C). This observation is particularly significant because the classical invagination model cannot generate single plasma membrane barriers between adjacent cytoplasmic domains. Instead, independent extension of severed sister membranes could explain the formation of cytoplasm-immersed membranes. To further test this hypothesis, we traced 12 cytoplasm-embedded membranes, including those separating Cell 1 from Cells 2 and 3, and those separating Cell 4 from 3 (Fig. 3D). In all cases, the cytoplasmic regions flanking these membranes belonged to cytosolically interconnected sister cells. Together, these results demonstrate that *C. elegans* embryonic cytokinesis relies on detached sister membrane extension rather than invagination mediated by intact membranes.

Tracing from the severed edges back to their origins, we found that the sister membranes were frequently anchored side-by-side near the cytosol-immersed region

(Fig. 4, A to D). Within this region, gap junction plaques were often observed (57/94) at membrane contact sites (Fig. 4B), though their potential role in sister membrane cohesion is unclear. These contact sites alternated with regions where the two sister membranes separated, revealing lightly stained intercellular spaces in EM images. Beyond the anchored region, the separation between sister membranes became evident and each membrane exhibited the characteristic features of a typical plasma membrane—with one side facing the cytosol and the other exposed to the extracellular environment (Fig. 4D).

Cellular vesicles were observed near free membrane edges (Fig. 4, A to C). Some cytosol-immersed membrane tips appeared connected to vesicles (Fig. 4A), with instances of direct contact (Fig. 4B) and possible fusion events (Fig. 4, B and C). Vesicles also clustered along the anchoring area, as well as the separated sister plasma membranes (Fig. 4D). EM analysis revealed no morphological differences between vesicles associated with the cytosol-immersed region and those near conventional regions of the sister membranes (Fig. 4, B and D).

Analysis of a tri-nucleated cell during cytokinesis

To gain more comprehensive insight into membrane organization during cytokinesis, we further applied the AutoCUTS-SEM (automatic collector of ultrathin sections scanning electron microscopy) workflow (*9*) to acquire serial EM sections of a telophase cell. Through continuous tracing, we discovered that this cell actually contained three independent nuclei. We color-coded each membrane region according to its associated nucleus, with relative sizes estimated from EM sections to ensure proportional representation (Fig. 5A). The 3D model demonstrated that the division plane between the yellow and blue cells was roughly perpendicular to that between

the purple cell and the other two (Fig. 5A). The presence of three nuclei within a shared cytoplasm suggests that one of the daughter cells entered the next round of cell division without completing the previous one. This phenomenon—concurrent divisions—appears to be common in early *C. elegans* embryos, as our EM analysis identified more than 10 cells with three or four nuclei (fig. S1). For example, Fig. 3D shows an EM section of a cell containing four nuclei.

Using consecutive EM sections, we traced membrane integrity in this tri-nucleated cell. We found that this tri-nucleated cell was enveloped by three distinct plasma membranes, each containing a single rupture site. These three ruptures converged to form a "Y"-shaped exposed cytoplasmic region spanning >351 sections (21,060 nm; Fig. 5, A and B and Movie S2). Throughout these 351 consecutive sections, we detected no continuity between adjacent membranes, indicating that membrane independence had been established by this stage. Consecutive tracing further showed that the MOs—frequently observed in single EM sections (Fig. 1 and 2)—could arise from either the separation between sister membranes (Fig. 5C) or from separated edges of the plasma membrane within the same cell (Fig. 5D). Additionally, multiple openings within a single cell might represent different cross-sectional planes of a common membrane rupture (Fig. 5E).

In all three cells (where cytoplasmic separation was incomplete), the free membrane edges were in close proximity (marked by *; Fig. 5, F and G), suggesting they were in late cytokinesis and that membrane extension mediated by detached membranes could persist into this stage. Taken together, these findings demonstrate that this tri-nucleated cell was undergoing concurrent cytokinesis, with three detached membranes independently extending toward a common cytoplasmic region to achieve

cytoplasm individualization (Fig. 5H). A similar mechanism may operate in four-nucleated cells, in which two detached daughter membranes—without completing the last round of cell division—undergo further rupture, forming four granddaughter membranes. These membranes then extend independently to complete cell division (Fig. 5H).

Capturing the membrane rupture and independent extension of detached sister membranes in living embryos

While high resolution HPF-TEM analysis revealed widespread membrane discontinuities in early *C. elegans* embryos, this static imaging approach cannot capture dynamic membrane behavior. To investigate whether optical microscopy can visualize membrane ruptures and the movement of severed sister membranes, we employed a fluorescence-labeled membrane marker, GFP::PH(PLC1δ1) (see Methods and Materials for details). Our live imaging detected both putative membrane ruptures (fig. 6A) and free-ended sister membrane structures (Fig. 6, B and C), providing additional evidence that membrane rupture and independent extension of detached sister membranes underlie cytokinesis in *C. elegans* embryos.

Extracellular matrix layers seal the exposed cytoplasmic regions

Plasma membrane integrity is critical for cell survival, as disruptions can lead to cytoplasmic leakage, which, if extensive, results in cell death. However, widespread cytoplasmic leakage has not been observed in wild-type *C. elegans* embryos. Based on our EM observations, we suspect that eggshell components may seal cytoplasmic regions lacking membrane coverage. The *C. elegans* eggshell is composed of six distinct extracellular matrix layers (*10–14*). Among these, the fifth permeability

barrier layer (PBL), a lipid-rich structure, serves as the osmotic and permeability barrier for the developing embryo (*10*, *11*). Normally, the PBL encloses the peri-embryonic layer (PEL), which separates it from the embryonic plasma membrane (*10*, *11*) (Fig. 7, A to C). In contrast, in regions where the plasma membrane was absent, we observed the PBL adhering directly to the exposed cytoplasm (red triangles and dashed red lines, Fig. 7, A to C), bypassing the PEL. This phenomenon was also evident in other EM images (Fig. 1, D and E, and Fig. 2). PBL-mediated sealing is not always complete. When the PBL was not accessible or only loosely covered membrane-free regions, minor cytoplasmic leakage occurred (Fig. 7D). In cases where PBL sealing was ineffective or absent, cytoplasmic material appeared to be retained within a confined region, likely by the PEL (Fig. 7D). However, the mechanisms by which extracellular matrix components protect the exposed cytoplasmic region remain unknown.

Discussion

In this study, we found that the plasma membrane of *C. elegans* embryonic cells undergoes rupture as early as metaphase. Following this rupture, the detached sister membranes extend independently from each other to accomplish cytokinesis. This unexpected finding presents numerous intriguing questions for future investigation.

First, how widespread is this remarkable cytoplasmic division pattern among species? A defining feature of early *C. elegans* embryogenesis is its extremely rapid cell division. Except for the first embryonic cell division, which occurs at approximately 40 minutes after fertilization, cell cycles preceding gastrulation last 15-30 minutes, alternating between S and M phases (*3–6*). After the onset of gastrulation

(around the 28-cell stage), the cell cycles lengthen, though the extent varies between lineages. Membrane discontinuities could be detected in more advanced embryos, though their frequency decreased dramatically as development progressed (see Methods and Materials for details). Since longer cell cycles reduce the likelihood of capturing cells in division, future studies will be needed to determine whether the cytokinesis mechanism described here operates beyond the embryonic cleavage stage. Notably, the ultrastructural dynamics of plasma membrane integrity during cell division have not been explored in other species. We anticipate that our work will catalyze comparative studies across species, to test whether this mechanism represents a fundamental paradigm or a context-specific strategy. Nevertheless, our findings establish the first mechanistic framework to guide such investigations.

Our survey using single EM sections revealed that membrane discontinuities are widely distributed across cells with diverse nucleoid morphologies. Intriguingly, the relative size of membrane discontinuities appears to peak during metaphase (Fig. 1 and 2). In addition, the metaphase rupture seemed predominantly localized around the equatorial plane (Fig. 2), raising the possibility that a region-specific surge in membrane tension drives plasma membrane breakage during this stage. As mitosis progresses, the relative size of the rupture may diminish, but it persists at least until late cytokinesis. Notably, membrane rupture was observed in the tri-nucleated cluster in Fig. 5, within which all three cells contained membrane discontinuities and were in the late cytokinesis stage. This suggests that the membrane rupture that originated during the previous round of division likely persisted throughout the entire cell cycle of the next division. Hence, at least in cases of concurrent cytokinesis, membrane discontinuities can endure for the full duration of the cell cycle. Of note, when two rounds of cytokinesis occurred simultaneously, only a single continuous rupture was

observed (Fig. 5). This finding also suggests that the rupture from the second metaphase either merges with the initial rupture site or that a strategically positioned rupture from the first division facilitates both rounds of cytokinesis.

3D reconstruction revealed that the metaphase rupture did not fully bisect the cell membrane (Fig. 2). However, since neither our random EM survey nor continuous EM tracking provides exhaustive coverage, we cannot rule out the possibility that some ruptures may completely sever the membrane in certain cases. Regardless of whether the membrane is fully separated, the rupture generates two distinctive membranes. Because this rupture occurs as early as metaphase—before nuclear or cytoplasmic division—the independence of the plasma membranes may precede other major cellular markers in defining nascent daughter cells.

Following membrane rupture, the prospective sister membranes become separated, raising the question of how cytokinesis proceeds with severed membranes. Analysis of single EM sections revealed classical membrane invagination in only a few cases (6 out of 51; Fig. 3A). Notably, one such instance occurred during the transition from a one-cell to a two-cell embryo. This suggests that while a subset of *C. elegans* embryonic cells employs the membrane invagination and extension model, the majority do not. Interestingly, membrane discontinuities were observed in one-cell embryos (fig. S1), indicating that membrane rupture can co-occur with invagination. Alternatively, in dividing cells, the back-to-back invagination may be transient and may subsequently transition to free-ended extension. At present, distinguishing between these hypotheses remains challenging. A definitive resolution will likely require advanced imaging techniques capable of high-resolution, real-time visualization at the EM level.

Unlike the continuous back-to-back membrane arrangement, the lack of a persistent connection grants individual sister membranes additional independence. This independence likely enables the two membranes to extend in different directions when necessary, even allowing them to turn or rotate freely relative to one another. Noticeably, such autonomous movement may also explain the divergent orientations of sister membranes frequently observed in EM sections.

When the severed edges meet within individual daughter cells, complete cytoplasmic independence is achieved. The fusion of free-ended membranes seems to resemble plasma membrane repair, a process that seals disruptions in the bilayer (*15*). However, it is unclear whether similar mechanisms are involved in the final step of this detached-membrane-driven cytokinesis. In the classical invagination-extension model, the final stage of cytokinesis requires both membrane scission and fusion (*16*, *17*). By contrast, in this detached-membrane mode, cytokinesis proceeds without a continuous membrane. This raises several questions. Is membrane scission dispensable in this context? Could bypassing scission accelerate daughter cell separation? If so, might such a mechanism provide a selective advantage for the rapid cell proliferation essential during early embryonic development? More importantly, how does the newly discovered cytokinesis model redefine our current understanding of abscission in cytokinesis? These questions remain open and warrant further investigations.

Using a fluorescence-labeled membrane marker, we were able to detect the likely membrane ruptures and free-ended sister membrane structures in live cells (fig. S3). However, interpreting these fluorescence patterns has been technically and conceptually challenging. On one hand, the rapid kinetics of membrane extension and

the inherent motility of dividing cells in the developing embryo introduces spatiotemporal ambiguities. On the other hand—and perhaps more critically—the longstanding influence of the membrane invagination model of cytokinesis has profoundly shaped, and may have inadvertently constrained, our interpretation of membrane dynamics. This deeply ingrained paradigm has likely influenced experimental design by traditionally prioritizing observations that align with invagination-based mechanisms, while potentially causing ambiguous membrane structures—such as free-ended extensions—to be overlooked or dismissed as artifacts rather than explored as alternative mechanisms in data interpretation. Furthermore, this paradigm dependence extends to theoretical modeling, where computational approaches have largely been built upon invagination-centric assumptions, potentially limiting our conceptual framework of cytokinetic possibilities. Here, our application of HPF-TEM has enabled unprecedented ultrastructural examination of dividing cell surfaces, revealing a cytoplasmic division mechanism that not only challenges current thinking but also raises profound new questions about the plasticity of cytokinesis mechanisms. This discovery, while transformative, represents just the beginning: future studies combining advanced live-cell imaging, biophysical modeling, and genetic approaches will be crucial to fully unravel the mechanistic basis of this process, determine its conservation across species, and evaluate its potential implications for developmental biology and cell cycle regulation more broadly.

Methods and Materials

Examination of *C. elegans* embryonic cells

Wild-type N2 worms were cultured on OP50-seeded NGM plates at 22°C (*18*). To obtain images of early embryos, gravid hermaphrodites were collected and sectioned. At low magnification (×4000), individual embryonic cells were identified by the presence of a nucleus. In sections where the nucleus was not visible, cytoplasmic regions—whether covered or not covered by plasma membrane—were counted as individual cells if they were separated from surrounding cells. A total of 425 cells were examined (summarized in Fig. 1C), with one EM section analyzed per cell. For embryos with fewer than 10 cells (one or two rows of cells), every cell in the given section was examined. For embryos with three or more rows of cells, only cells at the periphery were analyzed. At higher magnification (×30,000), the entire surface of each cell was examined, revealing 159 cells with one or more membrane openings. Higher magnification improved the resolution of cytoplasmic continuity, reducing potential misidentification of multinucleated cells or interconnected cytoplasmic regions that might have been miscounted at lower magnification. A total of 60 early embryos were serially sectioned as completely as possible, with each embryo yielding at least 20 sections. While Fig. 1C presents summary data, images from additional sections were also used for further analyses. Since these additional sections may capture different cells, the total number of embryonic cells examined likely exceeds 425.

Additionally, we examined eight embryos laid outside the worm. Among these, four pre-comma stage embryos each contained at least one MO-positive cell. In another pre-comma stage embryo, no MOs were detected after examining 17 cells.

Analysis of one comma-stage embryo (19 cells examined) and two 1.5-fold-stage embryos (>30 cells analyzed each) revealed no MOs.

Identification of MOs

The entire cell surface of individual embryonic cells was examined using electron microscopy at 30,000× magnification. The isolated cytoplasmic regions without plasma membrane coverage were defined as MOs. Sites where the plasma membrane terminated and reappeared were marked as putative MOs. In regions lacking a plasma membrane, the PEL was absent, while the PBL typically extended over the exposed cytoplasmic surface. Plasma membranes often appeared wrinkled, whereas cytoplasmic regions covered by the PBL exhibited a smoother appearance. Smooth, non-plasma-membrane-covered regions overlaid by the PBL are readily identifiable as MOs. When exposed cytoplasm was not tightly covered by the PBL, cytoplasmic leakage—still confined to a specific area by the PEL—could also indicate a MO. Given the variable morphology and frequent cytoplasmic leakage, membrane discontinuity size could not serve as a reliable criterion for defining MOs. However, to ensure robustness in our analysis, we considered only linear membrane discontinuities exceeding 200 nm as genuine openings. Each membrane opening was unbiasedly examined at least three times. Only if all three assessments confirmed its presence was the identification finalized.

High-pressure freezing and transmission electron microscopy

Basic protocols for high-pressure freezing of a range of organisms, including *C. elegans*, have been described (*19–21*). Briefly, adult worms were loaded into carriers and cryofixed using a Leica Microsystems EM ICE high-pressure freezer, followed by automatic cooling in liquid nitrogen. The carriers used for freezing (Leica Microsystems, Germany; catalog nos. 16770153 and 16770152) were coated with a

non-stick layer of 1-hexadecene (Sigma-Aldrich). After high-pressure freezing (HPF), the samples were transferred under liquid nitrogen to a Leica AFS-2 freeze-substitution unit and incubated at −90°C for 72 h in a freeze-substitution solution consisting of acetone with 2% (wt/vol) osmium tetroxide and 2% (vol/vol) water. The temperature was then raised at a rate of 8°C/h for 4 h, held at −60°C for 12 h, increased again at 5°C/h for 6 h, held at −30°C for 10 h, and finally raised to 10°C at a rate of 4°C/h for 10 h. Samples were washed four times in acetone, stained with 1% uranyl acetate for 1 h, and rinsed three times with pure acetone. They were then infiltrated stepwise in increasing concentrations of SPI-Chem™ resin (2:1 resin:acetone for 3 h, 1:1 for 5 h), followed by two incubations in 100% fresh resin (4 h each). The samples were placed in fresh resin in embedding molds and polymerized in a 60°C oven for 3 days. Ultrathin sections (60 nm) were cut using a diamond knife (Diatome) on an ultramicrotome (Leica Ultracut UC7) and collected on slot copper grids (EMS). The sections were visualized using a Hitachi HT7700 transmission electron microscope operating at 80 kV. Images were recorded with a Gatan 832 (4k × 2.7k) CCD camera. Data from four independent preparations were analyzed in this study.

3D reconstruction

The metaphase 3D model was prepared using the following steps. First, resin blocks containing gravid adults were prepared via high-pressure freezing and freeze substitution. Continuous ultrathin sections (60 nm thick) were manually collected using a Leica UC-7 ultramicrotome and mounted on slot grids for TEM imaging. A total of 112 serial sections were collected, though 3 sections were lost due to obstruction, resulting in 822 TEM images. Among these, 105 sections contained metaphase-stage cell information. To examine the plasma membrane integrity, high-

magnification imaging was performed. Since a single high-magnification image could not cover the entire cell, multiple overlapping images were captured per section and stitched together using ImageJ to generate a complete composite image of the cellular morphology at each section. In total, 292 images were stitched. The 105 stitched images were then aligned using ImageJ, and 99 of these aligned images were used for 3D reconstruction using Imaris software. About a quarter of the cell lacked membrane discontinuities. For this portion, we estimated its size and shape based on EM sections to ensure proportional representation. Of note, single MOs smaller than 200 nm that appeared continuously across more than 3 consecutive sections were considered the endpoint of the membrane rupture. Based on this, the actual length of the membrane rupture could be underestimated at one end, while the other end was clearly defined.

The ultrastructural 3D study of the tri-nucleated cell was performed using an AutoCUTS device (*9*) and a Helios Nanolab 600i dual-beam scanning electron microscope (FEI). Adult worms were treated with high-pressure freezing, freeze-substitution, and embedding as described above. Subsequently, 351 serial sections (60 nm thick) were collected using the AutoCUTS device, and scanning electron microscopy imaging was performed. All datasets were analyzed using IMARIS 8 software. After Z-stacks were aligned, the membrane rupture was manually traced and reconstructed.

Live imaging of plasma membrane dynamics using GFP::PH

The plasma membrane was labeled using GFP::PH(PLC1δ1). The strain carrying this marker was obtained from the Caenorhabditis Genetics Center and was originally generated in Dr. Karen Faye Oegema's laboratory. Gravid adult hermaphrodites expressing this marker were collected and washed with M9 buffer. Embryos were then released from the gravid adult worms using a 1 mL syringe needle and

transferred onto a 2% agarose pad. Fluorescence imaging was performed on a Zeiss LSM-980 microscope with a 63×/1.42 oil objective. Only one embryo at a time was imaged, starting at the 2- to 4-cell stage. Images were acquired at 4 or 8-second intervals, with total imaging duration typically kept under 30 minutes to ensure embryo viability.

Acknowledgements

We thank the Center for Biological Imaging, Institute of Biophysics, Chinese Academy of Sciences (CAS) for technical support. This work was supported by grants from the National Key R&D Program of China (2024YFA1803401, 2021YFA0805802, and 2024YFA1306100) and the Natural Science Foundation of China (32170790 and 32321004).

Figure legends

Fig. 1. Membrane discontinuities in *C. elegans* embryonic cells.

(A) Schematic drawing of a metaphase cell and the classical membrane invagination model. (B) Schematic drawing of a metaphase cell with a ruptured plasma membrane and a cytokinesis model showing that the detached sister membranes mediate membrane extension in *C. elegans* embryonic cells. Plasma membrane is in light blue. Condensed chromosomes are in red. Nuclei are in purple. (C) Summary of the single EM section survey of plasma membrane continuity in *C. elegans* embryonic cells. Orange lines outline the plasma membranes. Solid gray circles/ellipses enclosed by dashed lines represent evenly stained nucleoid regions. Condensed chromosome structures are colored gray-blue. Light brown areas represent cytoplasmic regions. (D) Membrane discontinuities or openings (MO) (white dashed line) in a metaphase cell (MC). Enlarged views of the boxed regions (1, 2 and 3) are shown. Yellow arrows indicate the plasma membrane (PM). (E) Membrane openings (marked by 1 and 2) are detected in anaphase (AC) and other early embryonic cells; enlarged views of the MOs are shown (white dashed lines). All yellow arrows point from the interior of the cell toward the plasma membrane.

Fig. 2. Metaphase membrane rupture.

(A-D) Three-dimensional (3D) reconstruction of a metaphase cell. Representative EM images are shown in (A) and (B). By aligning and merging multiple EM images, a composite image capturing the entire cell in a single section was generated (C), which was then used for 3D reconstruction of the metaphase cell. Purple lines outline the plasma membranes. White dashed lines outline the exposed cytoplasmic region. Blue lines outline the condensed chromosome region. (D) The 3D reconstruction of the

metaphase cell. The plasma membrane (PM) and condensed chromosome region are displayed.

Fig. 3. Configuration of detached severed sister membranes.

(A) Representative image of a classical back-to-back membrane arrangement. (B) Representative image of detached severed sister membranes. Diagrams of the corresponding cytokinesis models are displayed on the right. (C) Tips of two detached sister membranes. (D) Cytosol-immersed single membranes separating the cytoplasmic regions of two adjacent cells. Plasma membranes (PM) are indicated by yellow arrows (A, B, and D) or blue lines. Asterisks indicate membrane tips.

Fig. 4. Cellular vesicles on detached sister membranes.

(A) A vesicle localized at the tip of a cytosol-immersed membrane. (B) Vesicles clustering near the cytosol-immersed region of sister membranes. Contact or fusion between vesicles and membranes is indicated. The rectangular inset shows an enlarged view of a gap junction (GJ) plaque. (C) Putative fusion events between vesicles and free-ended membranes. (D) Vesicles found near the separated sister membranes. Plasma membranes are in blue.

Fig. 5. Membrane rupture on a tri-nucleated cell.

(A) 3D model of a tri-nucleated cell showing the membrane rupture (black). (B) Reconstruction of the membrane ruptures and adjacent plasma membranes. Individual

membranes, each associated with a distinct nucleus, are color-coded (blue, yellow, and purple). (C and D) Membrane openings (MO, dashed white lines) arise either from separation between sister membranes (C) or between the severed membrane edges of the same cell (D). (E) In a single EM section, the multiple openings originate from the same rupture. (F and G) The opposing severed edges are close to each other in the yellow, purple and blue cells. Plasma membranes (PM) are indicated in blue. Asterisks indicate membrane tips. (H) Schematic diagram of the formation of cells with three or four nuclei.

Fig. 6. Detection of potential membrane disruptions by optical microscopy.

(A) Possible membrane rupture (*). (B) Two possible fast-extending free-ended sister membranes (*). Insets are enlarged views. (C) Possible free-ended edges of detached membranes, probably from multiple cells (*). Below are proposed models illustrating the membrane disruptions that could explain the anomalous GFP signals. Images were taken at 4-second intervals for (A and B) and 8-second intervals for (C). Green signal is GFP::PH(PLC1δ1).

Fig. 7. The exposed cytoplasmic regions are covered by extracellular matrix layers.

(A-C) The exposed cytoplasmic region is covered by the permeability barrier layer (PBL, red triangles and red dashed lines). PM, plasma membrane (yellow arrows and blue lines). The boxed region in (A) is enlarged in (B), and the boxed region in (B) is enlarged in (C). (D) The exposed cytoplasmic region can also be confined by the peri-embryonic layer (PEL).

Supporting Information Legends

fig. S1. The wide distribution of cells with membrane discontinuities in early *C. elegans* embryos.

(A) Schematic diagram of *C. elegans* embryogenesis. (B-N) Representative low-magnification EM images of early embryos within adult hermaphrodites. Red lines outline cells contain membrane openings. In (F), a tri-nucleated cell is marked with &. (L) and (M) show embryos during the transition from the one-cell to the two-cell stage.

fig. S2. Membrane discontinuities in late-stage *C. elegans* embryos.

(A) A membrane discontinuity (white box) is detected in a late-stage embryo after egg laying; an enlarged view showing the membrane opening (white dashed line) is displayed in (B). * indicates the condensed chromosome structure. Yellow arrows point to the plasma membrane.

fig. S3. Membrane discontinuities in cells during mitosis.

(A-C) Membrane discontinuities or openings (MO, white or black dashed lines) in cells at metaphase (A), anaphase (B) or telophase (C). Yellow arrows points to plasma membranes (PMs).

Movie. S1. 3D reconstruction of the metaphase cell in Fig. 2.

The plasma membrane is shown in red, the condensed chromosome is in blue, and leaked cytoplasm is in green.

Movie. S2. 3D reconstruction of the tri-nucleated cell in Fig. 5.

3D reconstruction of membrane ruptures and adjacent plasma membranes. Individual membranes, each associated with a distinct nucleus, are color-coded (purple, yellow, or blue).

1. T. D. Pollard, B. O'Shaughnessy, Molecular Mechanism of Cytokinesis. *Annu. Rev. Biochem.* **88**, 661–689 (2019).

2. K. S. Gerien, J.-Q. Wu, Molecular mechanisms of contractile-ring constriction and membrane trafficking in cytokinesis. *Biophys Rev* **10**, 1649–1666 (2018).

3. L. G. Edgar, J. D. McGhee, DNA synthesis and the control of embryonic gene expression in C. elegans. *Cell* **53**, 589–599 (1988).

4. U. Deppe, E. Schierenberg, T. Cole, C. Krieg, D. Schmitt, B. Yoder, G. Von Ehrenstein, Cell lineages of the embryo of the nematode Caenorhabditis elegans. *Proc. Natl. Acad. Sci. U.S.A.* **75**, 376–380 (1978).

5. J. E. Sulston, E. Schierenberg, J. G. White, J. N. Thomson, The embryonic cell lineage of the nematode Caenorhabditis elegans. *Developmental Biology* **100**, 64–119 (1983).

6. Z. Bao, Z. Zhao, T. J. Boyle, J. I. Murray, R. H. Waterston, Control of cell cycle timing during C. elegans embryogenesis. *Developmental Biology* **318**, 65–72 (2008).

7. L. Pintard, B. Bowerman, Mitotic Cell Division in *Caenorhabditis elegans*. *Genetics* **211**, 35–73 (2019).

8. "Modern Electron Microscopy Methods for C. elegans" in *Methods in Cell Biology* (Elsevier, 2012; https://linkinghub.elsevier.com/retrieve/pii/B9780123946201000047), pp. 93–149.

9. X. Li, G. Ji, X. Chen, W. Ding, L. Sun, W. Xu, H. Han, F. Sun, Large scale three-dimensional reconstruction of an entire Caenorhabditis elegans larva using AutoCUTS-SEM. *Journal of Structural Biology* **200**, 87–96 (2017).

10. S. K. Olson, G. Greenan, A. Desai, T. Müller-Reichert, K. Oegema, Hierarchical assembly of the eggshell and permeability barrier in *C. elegans*. *Journal of Cell Biology* **198**, 731–748 (2012).

11. G. Benenati, S. Penkov, T. Müller-Reichert, E. V. Entchev, T. V. Kurzchalia, Two cytochrome P450s in Caenorhabditis elegans are essential for the organization of eggshell, correct execution of meiosis and the polarization of embryo. *Mechanisms of Development* **126**, 382–393 (2009).

12. C. A. Rappleye, A. R. Paredez, C. W. Smith, K. L. McDonald, R. V. Aroian, The coronin-like protein POD-1 is required for anterior-posterior axis formation and cellular architecture in the nematode Caenorhabditis elegans. *Genes &*

Development **13**, 2838–2851 (1999).

13. E. Schierenberg, B. Junkersdorf, The role of eggshell and underlying vitelline membrane for normal pattern formation in the early C. elegans embryo. *Roux's Arch Dev Biol* **202**, 10–16 (1992).

14. K. K. Stein, The C. elegans eggshell. *WormBook*, 1–36 (2018).

15. N. W. Andrews, M. Corrotte, Plasma membrane repair. *Current Biology* **28**, R392–R397 (2018).

16. J. P. Fededa, D. W. Gerlich, Molecular control of animal cell cytokinesis. *Nat Cell Biol* **14**, 440–447 (2012).

17. R. A. Green, E. Paluch, K. Oegema, Cytokinesis in Animal Cells. *Annual Review of Cell and Developmental Biology* **28**, 29–58 (2012).

18. S. Brenner, THE GENETICS OF *CAENORHABDITIS ELEGANS*. *Genetics* **77**, 71–94 (1974).

19. R. M. Weimer, "Preservation of *C. elegans* Tissue Via High-Pressure Freezing and Freeze-Substitution for Ultrastructural Analysis and Immunocytochemistry" in *C. Elegans* (Humana Press, New Jersey, 2006; http://link.springer.com/10.1385/1-59745-151-7:203)vol. 351, pp. 203–222.

20. K. McDonald, "Cryopreparation Methods for Electron Microscopy of Selected Model Systems" in *Methods in Cell Biology* (Elsevier, 2007; https://linkinghub.elsevier.com/retrieve/pii/S0091679X06790021)vol. 79, pp. 23–56.

21. L. Manning, J. Richmond, "High-Pressure Freeze and Freeze Substitution Electron Microscopy in C. elegans" in *C. Elegans*, D. Biron, G. Haspel, Eds. (Humana Press, Totowa, NJ, 2015; https://link.springer.com/10.1007/978-1-4939-2842-2_10)vol. 1327 of *Methods in Molecular Biology*, pp. 121–140.

Figure1

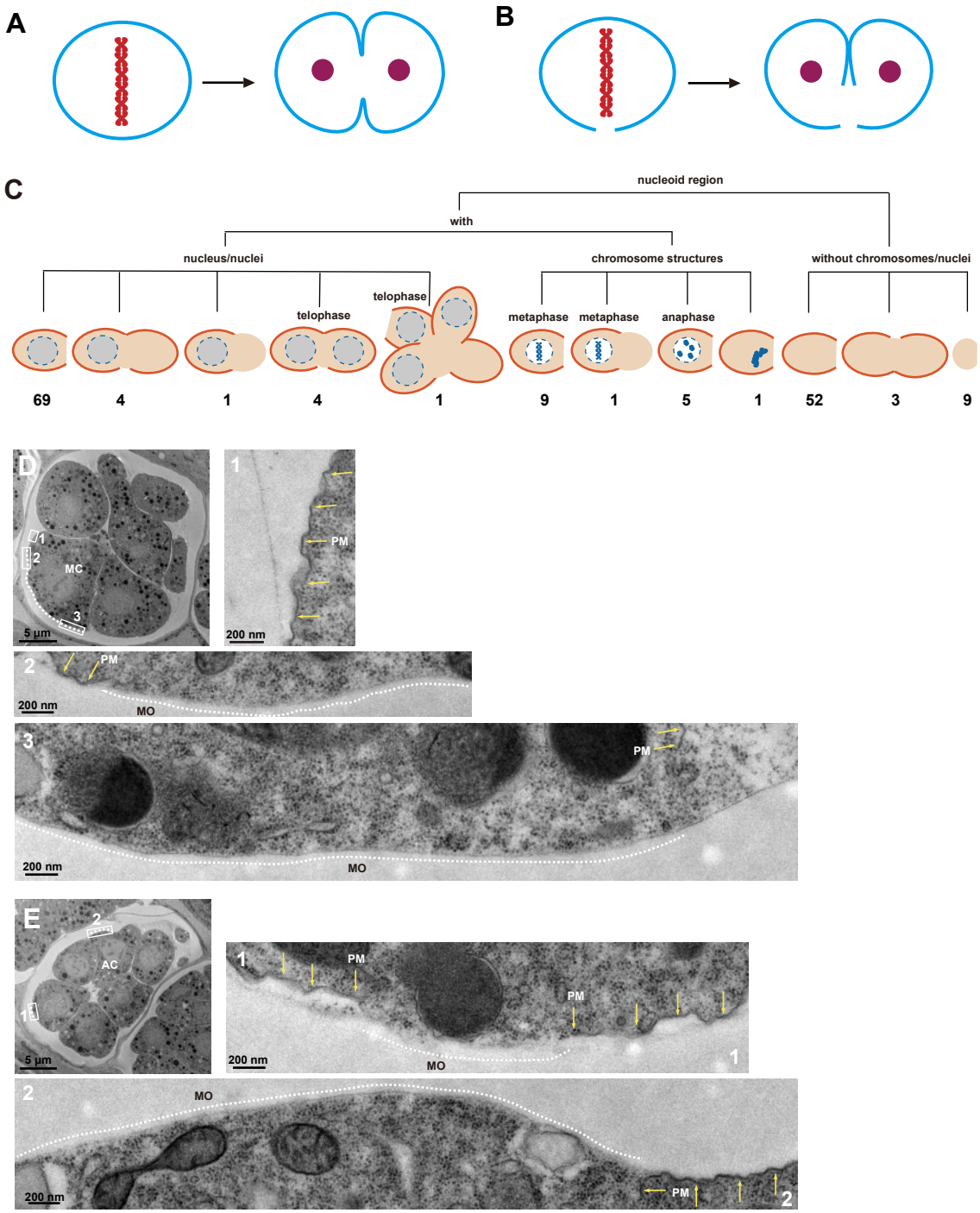
A
B
C
nucleoid region
with
nucleus/nuclei
chromosome structures
without chromosomes/nuclei
telophase
telophase
metaphase
metaphase
anaphase
69
4
1
4
1
9
1
5
1
52
3
9
D
MC
PM
MO
5 µm
200 nm
E
AC
PM
MO
5 µm
200 nm

Figure 2

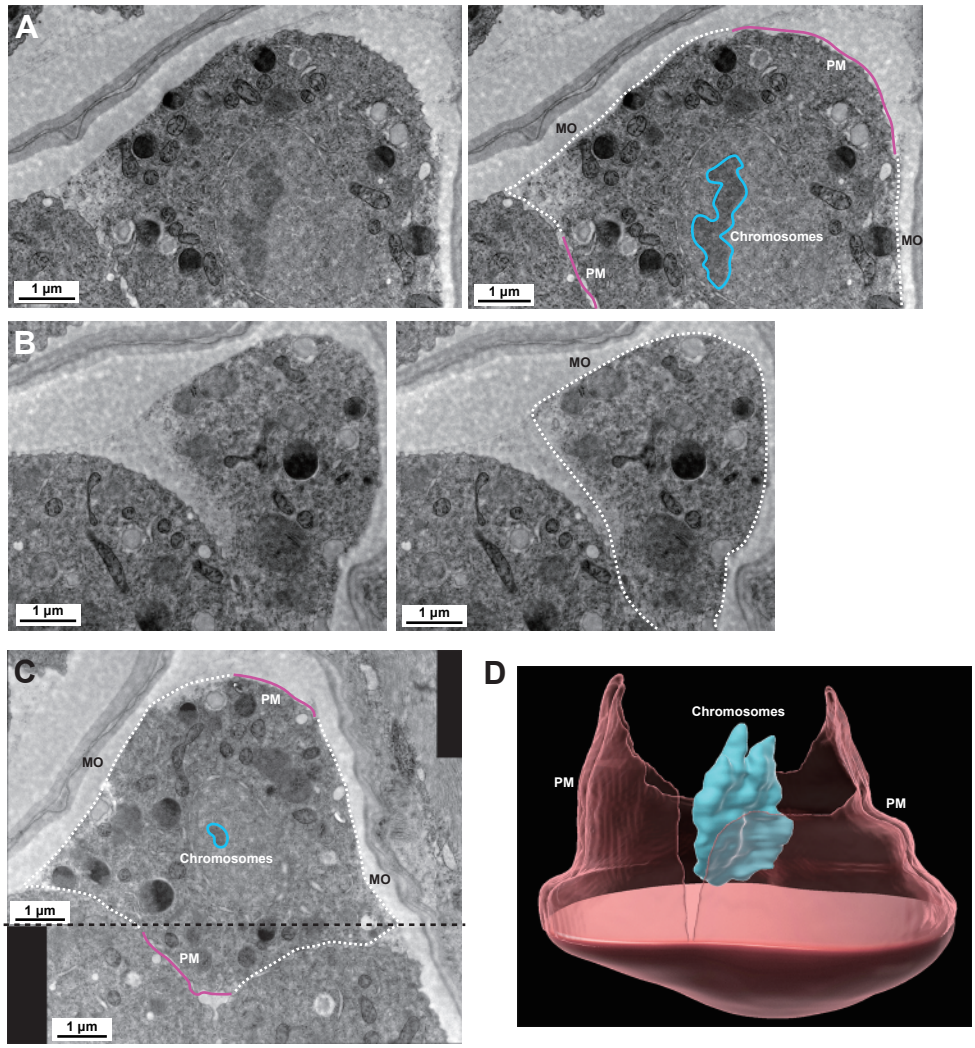
A
1 µm
PM
MO
Chromosomes
MO
PM
1 µm
B
1 µm
MO
1 µm
C
PM
MO
Chromosomes
MO
1 µm
PM
1 µm
D
Chromosomes
PM
PM

Figure 3

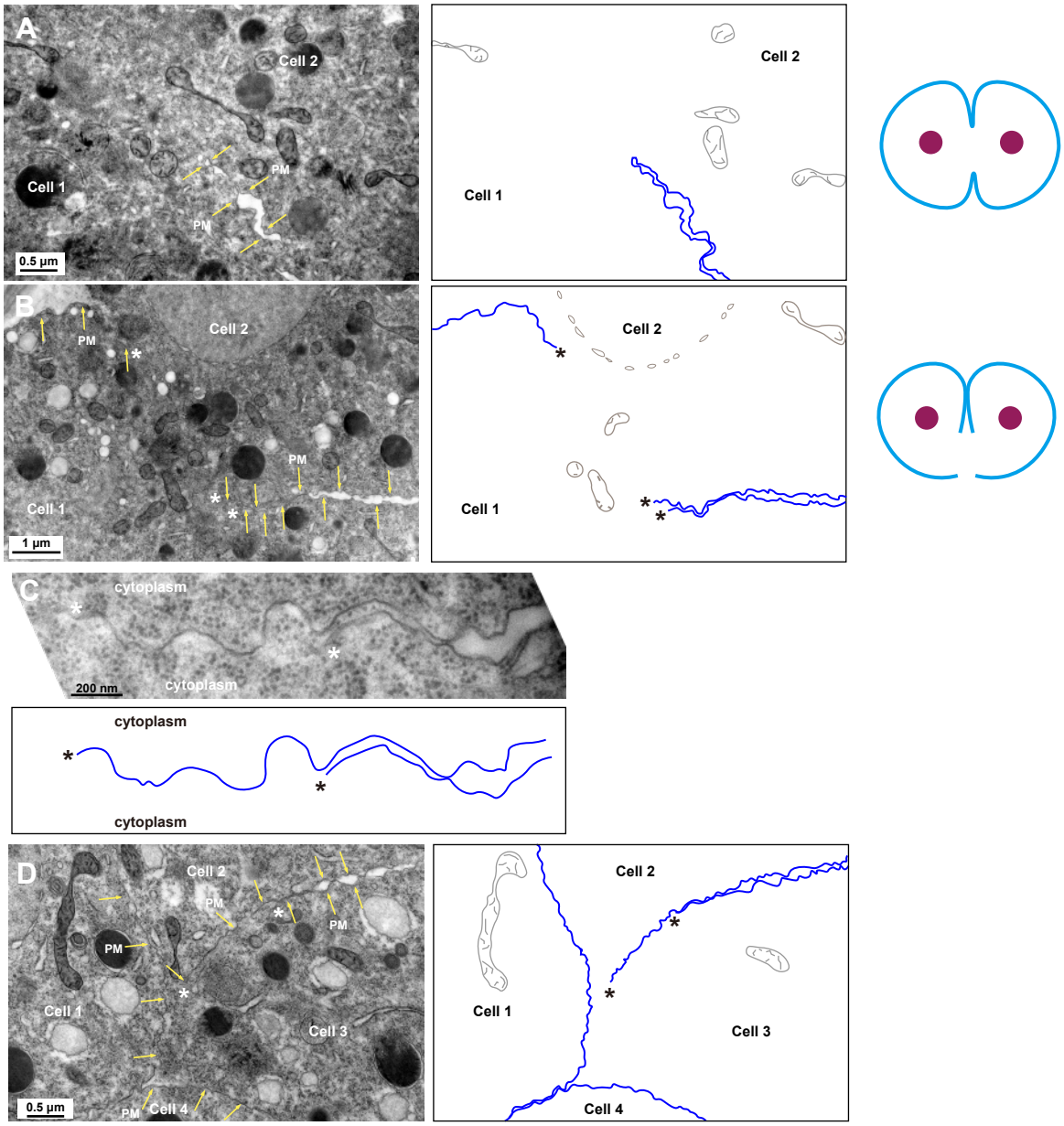
A
Cell 1
Cell 2
PM
PM
0.5 µm
Cell 2
Cell 1
B
PM
Cell 2
PM
Cell 1
1 µm
Cell 2
Cell 1
C
cytoplasm
cytoplasm
200 nm
cytoplasm
cytoplasm
D
Cell 2
PM
PM
PM
Cell 1
Cell 3
0.5 µm
PM
Cell 4
Cell 2
Cell 1
Cell 3
Cell 4

Figure 4

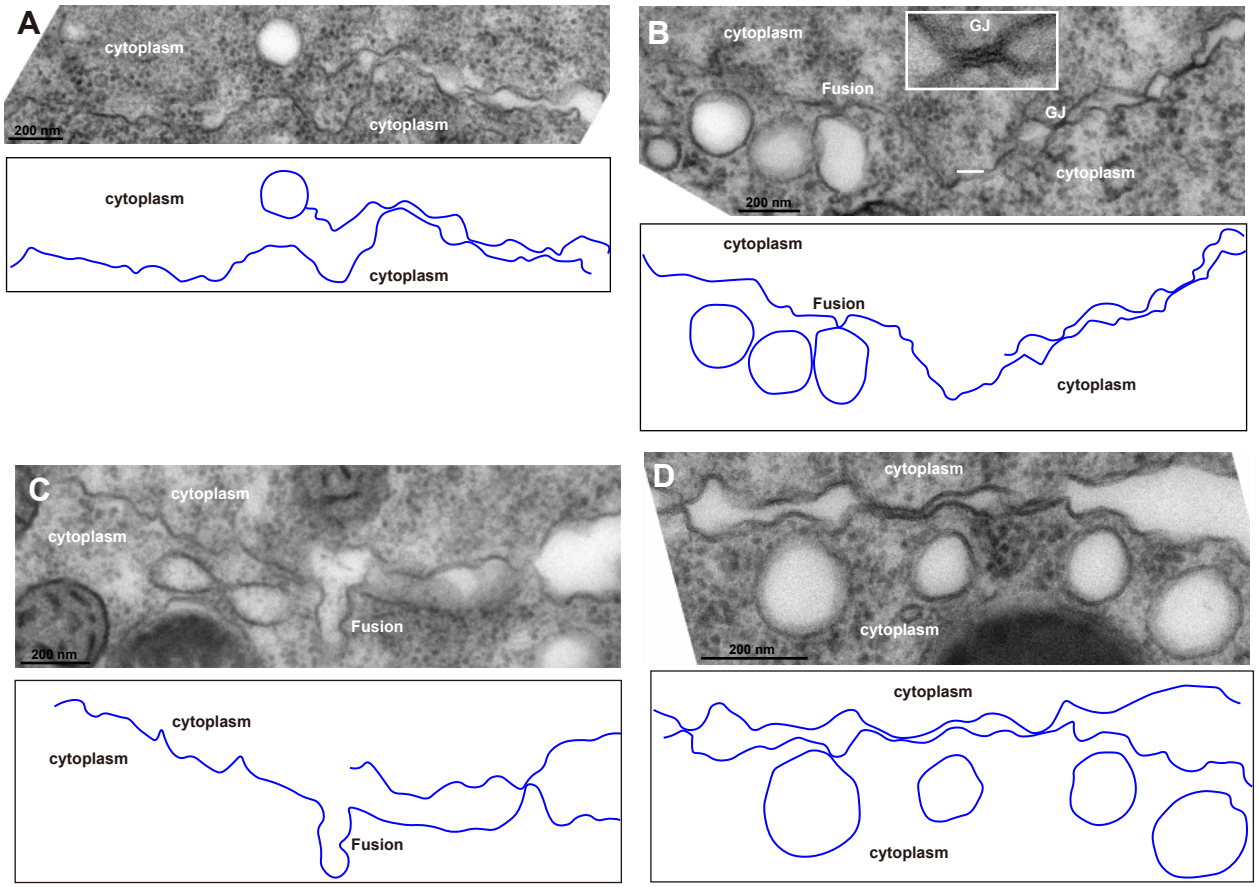
A
cytoplasm
cytoplasm
200 nm
cytoplasm
cytoplasm
B
cytoplasm
GJ
Fusion
GJ
cytoplasm
200 nm
cytoplasm
Fusion
cytoplasm
C
cytoplasm
cytoplasm
Fusion
200 nm
cytoplasm
cytoplasm
Fusion
D
cytoplasm
cytoplasm
200 nm
cytoplasm
cytoplasm

Figure 5

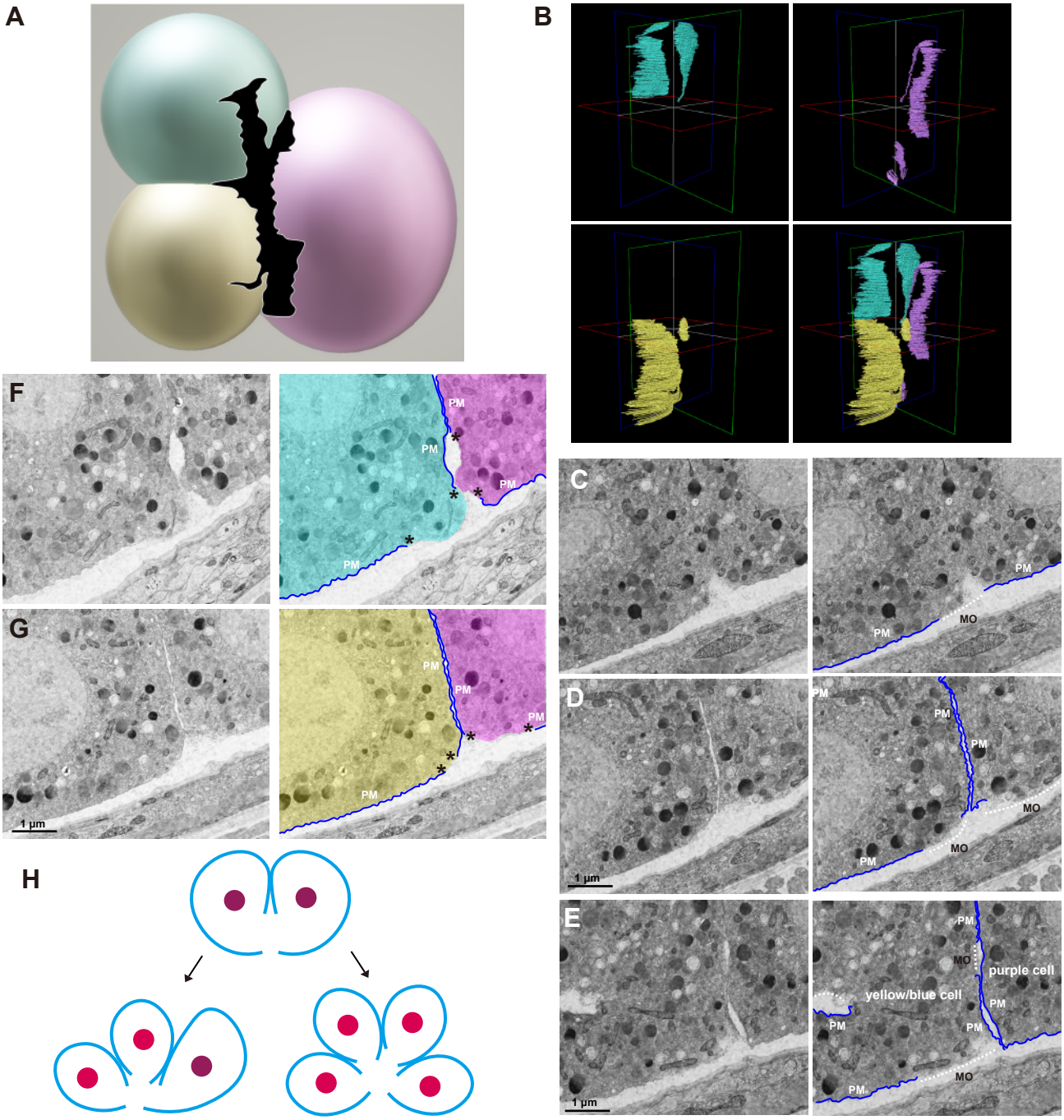

Figure 6

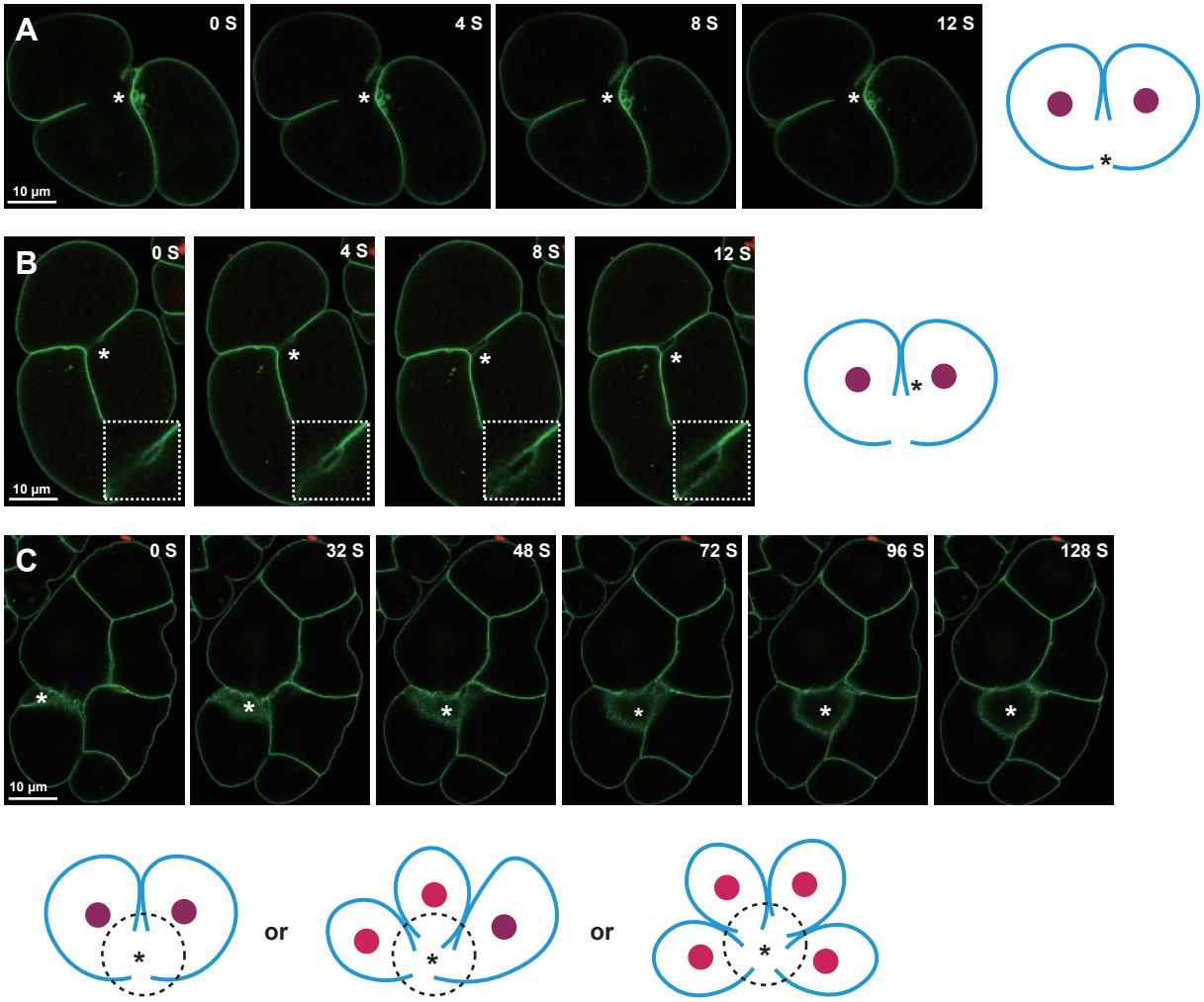
A
0 S
4 S
8 S
12 S
10 µm
B
0 S
4 S
8 S
12 S
10 µm
C
0 S
32 S
48 S
72 S
96 S
128 S
10 µm
or
or

Figure 7

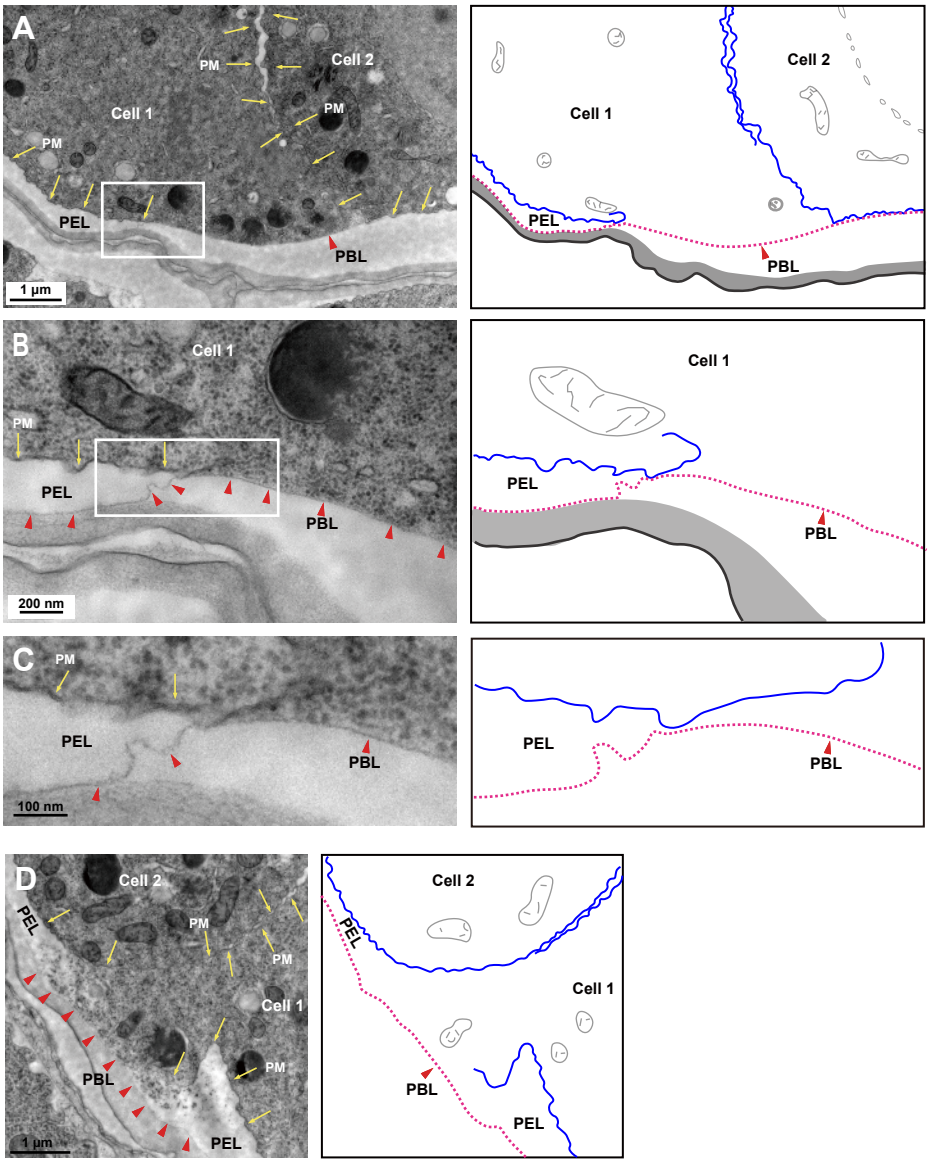
A
PM
Cell 2
Cell 1
PM
PM
PEL
PBL
1 µm
Cell 2
Cell 1
PEL
PBL
B
Cell 1
PM
PEL
PBL
200 nm
Cell 1
PEL
PBL
C
PM
PEL
PBL
100 nm
PEL
PBL
D
Cell 2
PEL
PM
PM
Cell 1
PM
PBL
PEL
1 µm
Cell 2
PEL
Cell 1
PBL
PEL

Sup Figure 1

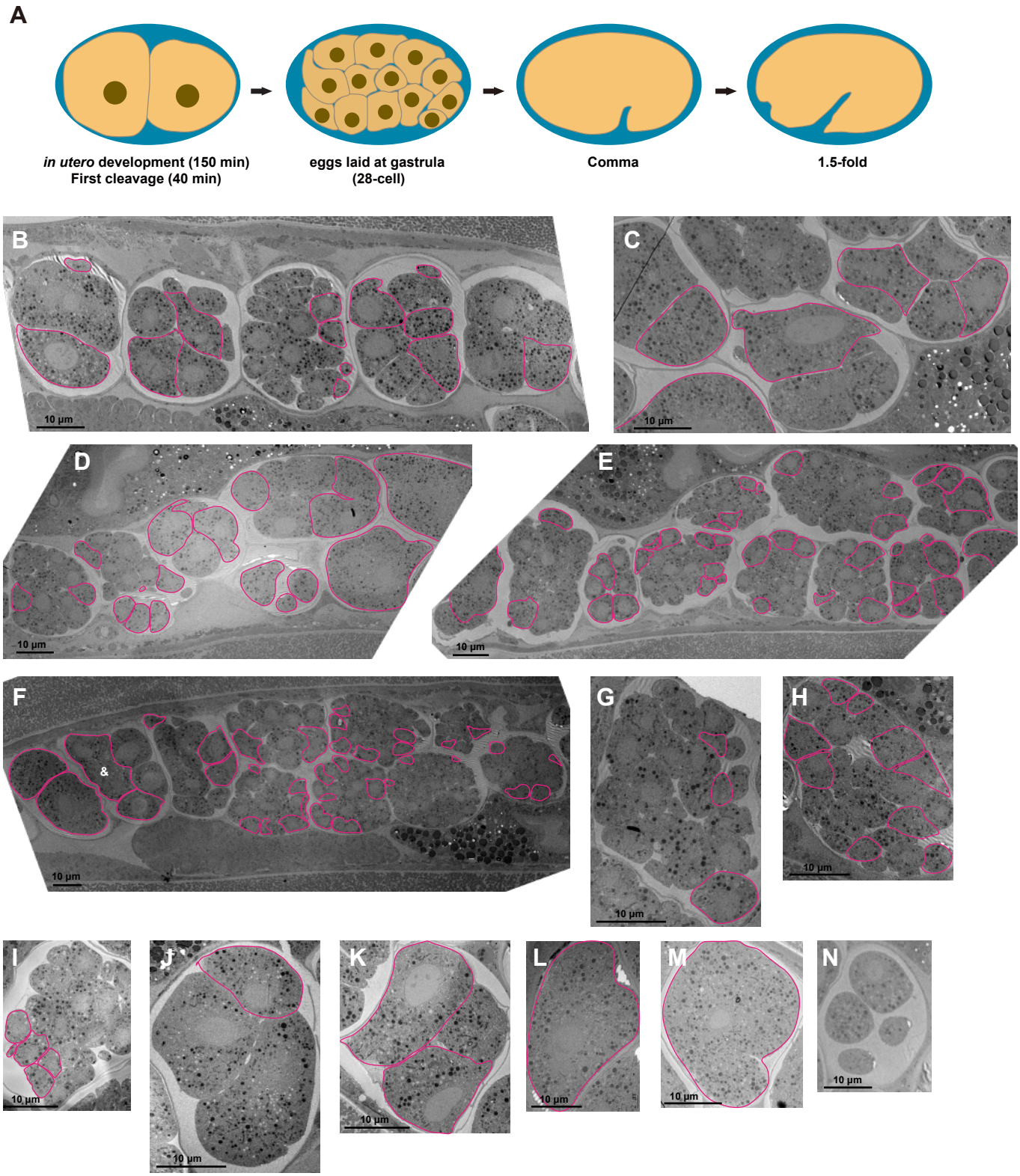
A
in utero development (150 min)
First cleavage (40 min)
eggs laid at gastrula
(28-cell)
Comma
1.5-fold
B
C
D
E
F
&
G
H
I
J
K
L
M
N
10 µm

Sup Figure 2

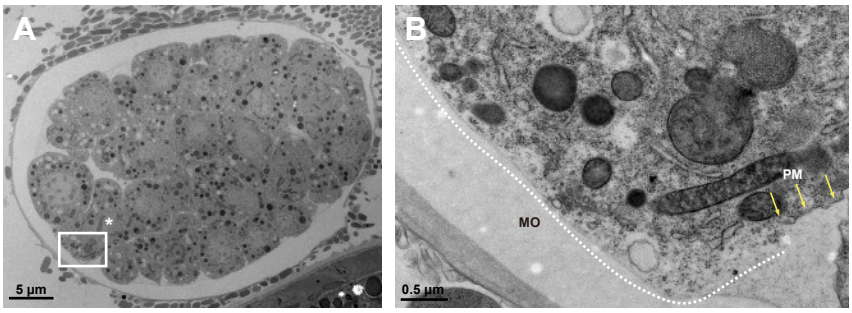

Sup Figure 3

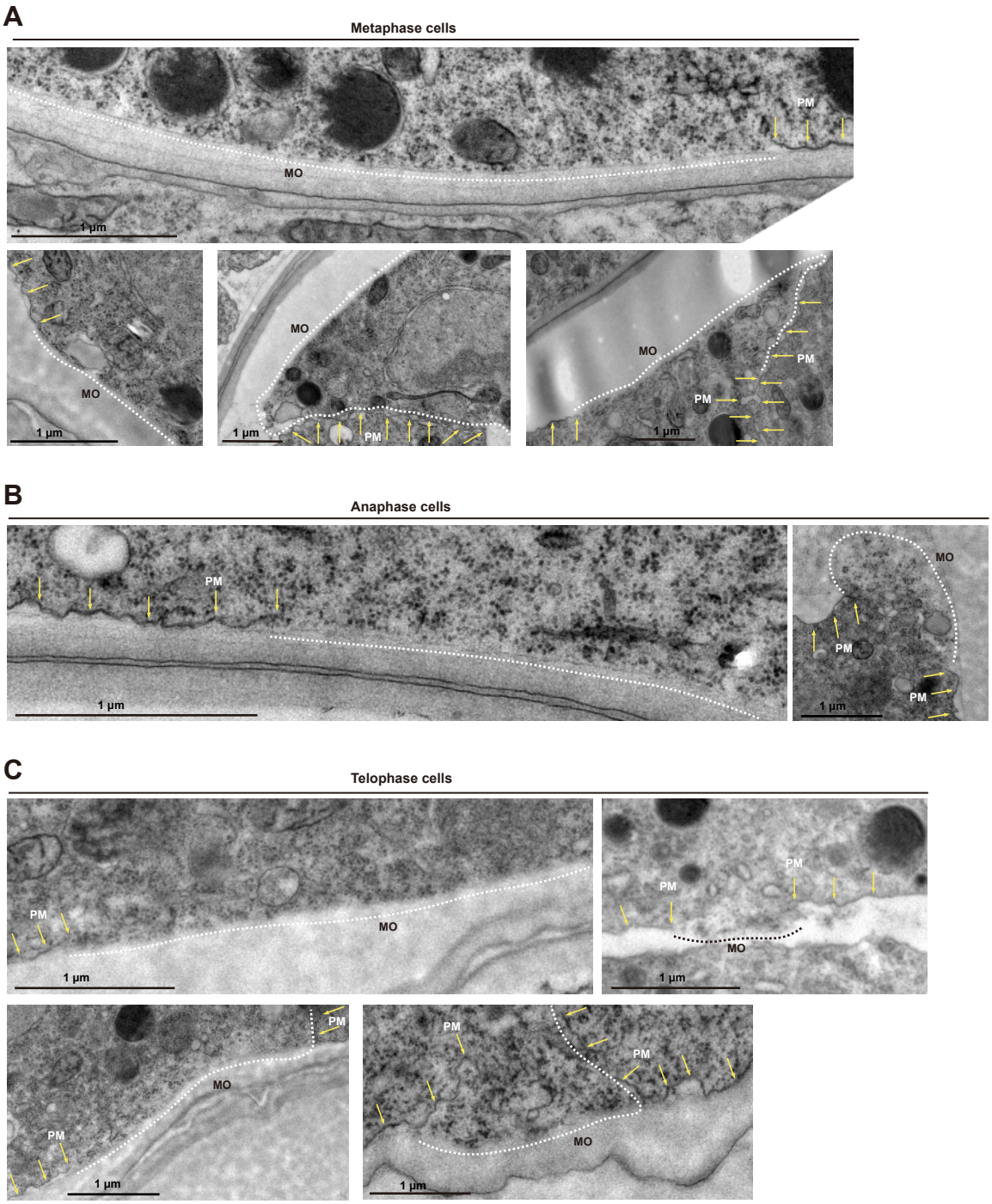
A
Metaphase cells
PM
MO
1 µm
MO
1 µm
MO
1 µm
PM
MO
PM
PM
1 µm
B
Anaphase cells
PM
1 µm
MO
PM
PM
1 µm
C
Telophase cells
PM
MO
1 µm
PM
PM
MO
1 µm
PM
MO
PM
1 µm
PM
PM
MO
1 µm